Journal of Sensor Science and Technology
Vol. 32, No. 6 (2023) pp. 391-402
http://dx.doi.org/10.46670/JSST.2023.32.6.391
pISSN 1225-5475/eISSN 2093-7563

Review of Low-Dimensional Nanomaterials for Blue-Light Emission

Won Kook Choi[1,+]

Abstract

Low-dimensional (zero-dimensional (0-dim), 2-dimensional (2-dim)) nanoparticles, such as chalcogenide compound semiconductors, III-V semiconductors, transition metal dichalcogenides (TMDs), II-VI semiconductors, nanocarbons, hybrid quantum dots (QDs), and perovskite QDs (PQDs), for which blue light emission has been observed, are reviewed. Current synthesis and device fabrication technologies as well as their prospective applications on next-generation quantum-dot-based light-emitting diodes are discussed.

Keywords: Low-dimensional nanoparticle, Quantum confinement, QDs, Blue emission, LEDs, Perovskite QDs

1. INTRODUCTION

Quantum dots (QDs) are small particles composed of tens to hundreds of atoms. They are known as semiconductors that are larger than atoms and molecules but smaller (<10 nm) than general nanoparticles (NPs) (10-100 nm). When the size (d) becomes smaller than Bohr's exciton radius owing to the quantum confinement effect, the electron energy level rises and the band gap, $E_{g,QDs}=E_g + (h^2\pi^2n^2/8md^2)$, increases. Thus, it is possible to adjust the bandgap and achieve emission up to the near infrared and ultraviolet regions (Fig. 1). Because the full width at half maximum (FWHM) of the emission spectrum is very small and the purity is excellent, excellent color rendering index (CRI), wide color gamut, high brightness with low turn-on voltage, ultrathin form factor, and quantum yield can be realized up to the theoretical value [1,2]. Therefore, quantum-dot light-emitting diodes (QLEDs) have emerged as promising candidates for next-generation displays. Wet process through dispersion in various solvents by combining with organic ligands can be easily performed on QLEDs. They are considered a next-generation flat panel display material after organic light-emitting diodes (OLED), with the exception of photo-absorption, photo-conversion, photoelectrochemical cells, and quantum Q-bits operating at ambient environment. To date, various QDs have been implemented in the form of low-dimensional nanomaterials, which can be broadly classified into zero-dimensional (0-dim) and two-dimensional (2-dim) materials. As 0-dim QDs, binary QDs consist of semiconductor materials II–VI (CdSe, ZnS, and ZnO), III–V (InAs and InP), and IV–VI (PbS and PbTe) [3-7]. Despite their bright luminescence and high photo- and colloidal stability, the toxicity of some elements (Cd, Pb, Se, and Hg) and precursors, time-consuming synthesis processes, complex purification processes, and laborious surface hydrophilization limit their use. QDs with ternary compositions I–III–VI_2 (I = Cu, Ag; III = In, Al, Ga; VI = S, Te, Se) possess a broad absorption spectrum and high photostability. However, they are not composed of toxic elements and have a characteristic non-stoichiometry that offers new possibilities for their use [8]. These nanomaterials have mainly been used to synthesize colloidal QDs (CQDs) by methods such as hot injection [9], gas-phase precursor synthesis [10], and microfluidic reactors [11,12]. As 2-dim QDs, 2-dim transitional metal dichalcogenides (TMDs) combined by weak van der Waals (vdWs) interactions are of interest because of their unique electrical and optical properties. Other 2-dim nanocarbons, such as graphene QDs (GQDs), graphene oxide QDs (GO-QDs), and carbon dots (C-dots), have been investigated as potential candidates for visible emission. Hybrid QDs of ZnO/nanocarbons or ZnO/functionalized polyaromatic carbons (f-PAHs) and perovskite quantum dots (PQDs) have emerged as emissive nanomaterials. White-emission flat displays have been accomplished using the excitation of red and green phosphors by either blue LEDs (micro-LEDs) or blue OLEDs (white OLEDs). Highly efficient blue-emissive QDs are in high demand for future QD-based self-emissive electroluminescent (EL) displays. Hence,

[1] Center for Optoelectronic Materials and Devices, Korea Institute of Science and Technology, Seoul 02792, Republic of Korea
[+]Corresponding author: wkchoi@kist.re.kr
(Received: Sep. 18, 2023, Revised: Oct. 5, 2023, Accepted: Oct. 6, 2023)

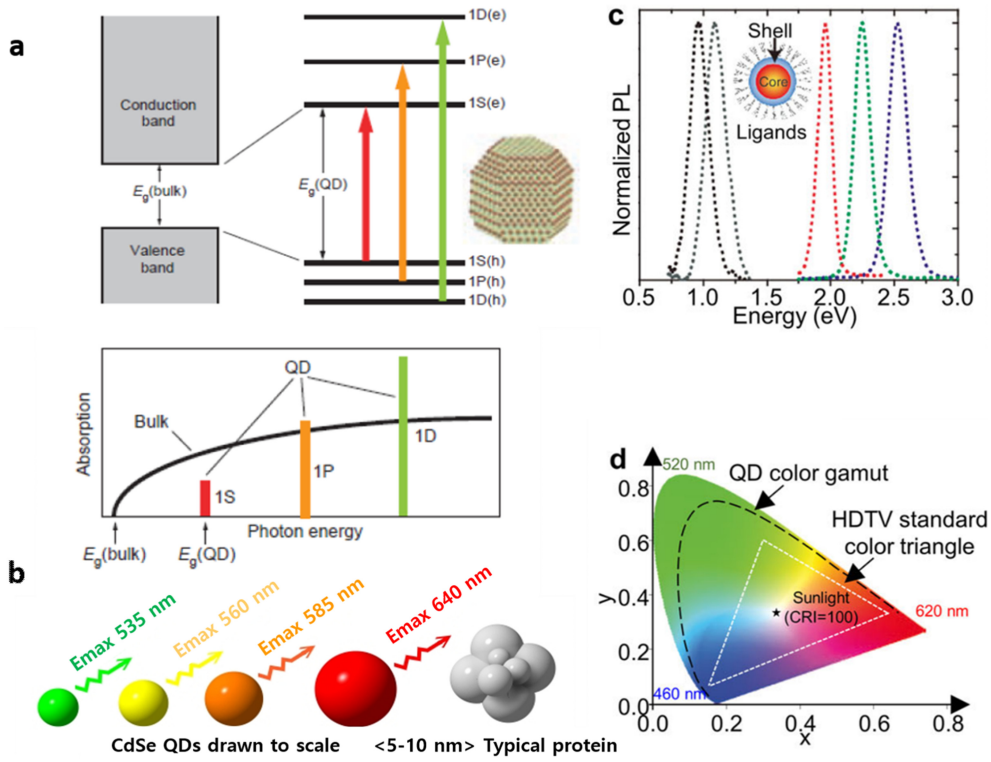

Fig. 1. (a) Increased bandgaps of E_g (QDs) vs E_g (bulk) and (b) modulated emission by quantum confinement effect. (c) High color purity (d) Large color gamut of QDs.

state-of-the-art low-dimensional blue luminescent nanomaterials are reviewed in terms of material and device development technology.

2. Low-Dimensional QDs

2.1 Inorganic QDs

2.1.1 II–VI and III–V Binary QDs

The high thermal stability of inorganic QDs with high color purity (FWHM: approximately 30 nm), high brightness (approximately 200,000 cd m^{-2}), and low operating voltage ($V_{turn-on}$ <2 V) enables prolonged lifetime and durability of flat-panel displays compared to commercialized high-definition television [13-15]. Type I core/shell materials, such as CdSe/ZnS, are commonly adopted in QLEDs owing to the passivation of interface defects and confinement of excitons to the cores, which greatly improves both the photoluminescence quantum yield (PLQY) and external quantum efficiency (EQE) by up to 70–95%. In addition, an increase in the shell thickness enhances the EL efficiency by reducing the blinking suppression of the charge fluctuation or enhancing the PLQY. QDs with ZnSe-rich intermediate shells demonstrate superior EL performance compared to those with CdS-rich shells owing to the lower charge injection barrier. [16]

Cd(Zn)Se(S)-alloyed QLEDs [17-19] including CdSe/ZnS QDs (470 nm) [20], inverted $Cd_{1-x}Zn_xS$@ZnS (437 nm) [21], CdZnS/ZnS core/ shell QDs (452 nm) [22], and CdSe/CdS (455 nm) QDs [23] exhibited blue EL of 437–477 nm, EQE of 1.7–19.8%, brightness of 2250–62 600 cd m^{-2}, and lifetime T_{50} (time required for the brightness to decrease to 50% of the initial value, h@100 cd m^{-2}) of 16–10 000 h.

Owing to the European Union (EU)'s Restriction of the use of the certain hazardous substances (RoHS), the use of heavy toxic elements such as Cd and Pb is strongly restricted. III-V InP QDs covering the entire visible range and possessing high PLQY, were developed as promising alternatives to Cd-chalcogenide blue-emissive QDs of InP/GaP/ZnS QDs (460−490 nm) [24]. They exhibited an EL of 488 nm, a record brightness of 3120 cd m^{-2}, and EQE of 1.01% [25].

Among II-VI semiconductors, ZnO and ZnSe have been extensively investigated as blue-emissive QDs. When ZnO QDs were synthesized, intrinsic defects, such as oxygen vacancies (V_o) and Zn interstitials (Zn_i) generating green and yellow emissions, were hardly controlled. To achieve blue emission, hybrid ZnO

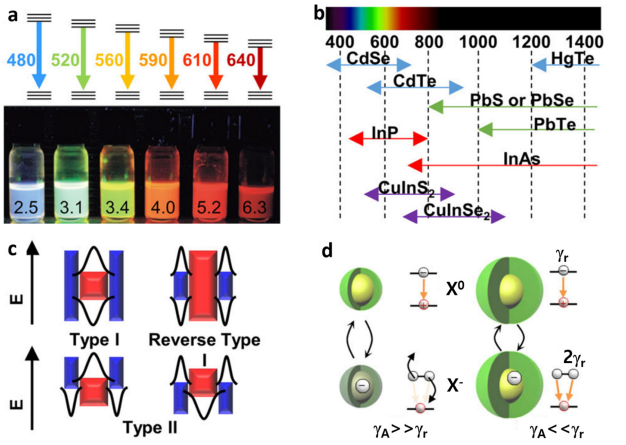

Fig. 2. (a) Photograph of solutions of different size CdSe QDs showing different visible emission. (b) Spectra ranges of various inorganic binary QDs. Reprinted with permission from Ref. [17] Copyright (2010) Wiley. (c) Electronic band structure of Type I, II, and reverse type QDs. (d) Comparison to carrier dynamics of core/shell QDs with thin or thick shells.

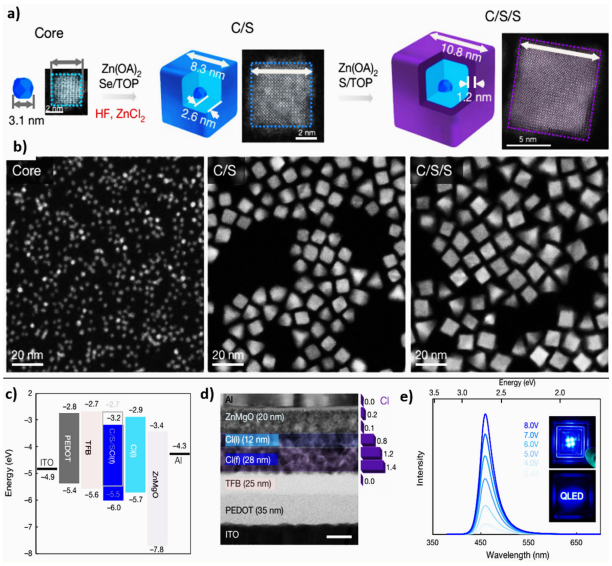

Fig. 3. (a) ZnTeSe/ZnSe/ZnS core-shell-shell QDs, (b) HRTEM images, (c) electronic diagram of QLEDs, (d) cross-sectional QD-LEDs, and (e) EL spectra. Reprinted with permission from Ref. [26] Copyright (2020) Nature Publishing Group.

QDs were fabricated by conjugating with nanocarbons or f-PAHs. Recently, optimized Te-doped ZnSe ($ZnTe_xSe_{1-x}$)-based ZnTeSe/ZnSe/ZnS core-shell-shell QLEDs successfully demonstrated blue luminescence at 457 nm, an EQE=20.2% with brightness of 88 900 cd m^{-2} (close to the theoretical limit), and the longest lifetime of T_{50}=15 850 h [26] (Fig. 3). As shown in Fig. 4, a blue gap exists between the InP and ZnSe QDs. InP QDs must be fabricated at sizes smaller than 1 nm in diameter and the poor color purity (FWHM ≥ 35 nm) must be overcome. Further, the high price of In remains an unresolved hurdle. In addition, the limitations of the use of ZnSe for the growth of QDs that emit pure blue color lies in its wide band gap of 2.7 eV. However, they can be overcome by alloying it with zinc telluride (ZnTe), which has a low band gap of 2.25 eV.

2.1.2 I–III–VI_2 Ternary QDs.

I–III–VI_2 semiconductors represent a new class of luminescent materials that combine unique optical and electronic properties, while exhibiting low toxicity compared to conventional cadmium-based QDs. I–III–VI_2 (I = Cu, Ag; III = In, Al, Ga; VI = S, Te, Se), high photostability, and large non-stoichiometry. I–III–VI_2 QDs exhibit a forward bandgap with a width of 1.5 eV (Cu-In-S), 1.05 eV (Cu-In-Se), 1.87 eV (Ag-In-S), and 1.2 eV (Ag-In-Se), which are unsuitable for blue emission [27]. The optical properties of $CuInS_2$ (CIS) and $AgInS_2$ (AIS)are studied in detail. Another fundamental drawback of I–III–VI_2 QDs is the broad FWHM of

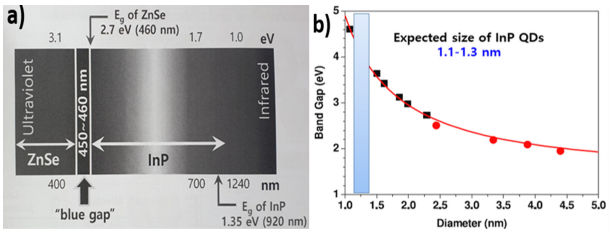

Fig. 4. (a) Blue gap between InP and ZnSe QDs. (b) band gap as a function of the size of InP QDs.

the PL (approximately 100 nm), which is disadvantageous for applications in fluorescent devices [28].

2.2 Nanocarbons

0-dim fullerene (C_{60}, C_{70}) or carbon dots (C-dots), one-dimensional (1-dim) carbon nanotubes, and 2-dim graphene are allotropes with spherical, cylindrical, two-dimensional nanostructures, and typical nanocarbons. When 2D graphene becomes size-controlled into a few tenth-nanometer GQDs and edge-functionalized GO-QDs, finite-sized 0D GQDs or GO-QDs exhibit a bandgap owing to quantum confinement (Fig. 5). The PL of GQDs and GO-QDs depends on the physical size and shape, as well as the chemical environment and surface functionality, such as the pH and solvent. To date, 0D nanostructures such as metal NPs and nanoclusters [29-31], metal sulfide QDs [32,33], and carbon nanodots (NDs) [34-36] have been extensively reported.

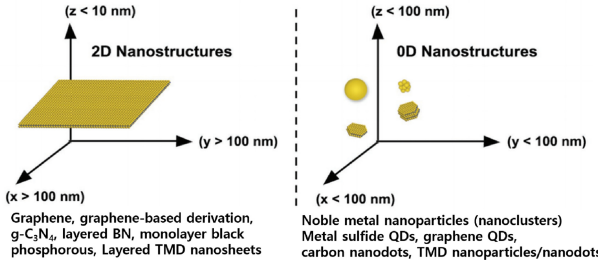

Fig. 5. Schematic of dimensionality from 2D to 0D.

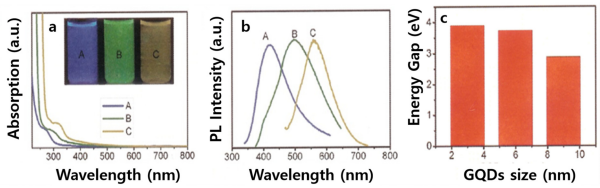

Fig. 6. (a) UV-Vis absorption spectra, (b) PL spectra, and (c) band gaps of GQDs synthesized by oxidation and cutting of carbon fibers. Reprinted with permission from Ref. [44] Copyright (2012) ACS Publications.

2.2.1 GQDs

Graphene, a Dirac cone crystal, has a zero bandgap, while graphene nanoribbons have bandgaps of up to approximately 0.4 eV. However, the energy gap of GQDs decreases as approximately 1/L [37]. Here, L is the average size of GQDs, which can be controlled up to approximately 3 eV, which is promising for photonic devices. GQDs can be synthesized using either chemical synthetic bottom-up methods, such as stepwise organic synthesis, precursor pyrolysis, and metal-catalyzed decomposition, or chemical cutting top-down methods, such as chemical ablation, nanolithography, electrochemical synthesis, chemical exfoliation, nanotomy-assisted exfoliation, and ultrasonic shearing. The optoelectronic properties of carbon materials are crucially determined by the π-π* transition of the sp^2 bond existing in the band gap of the σ-σ* transition of the sp^3 bonding [38-40] The strong peak generally observed at approximately 275 nm (approximately 4.5 eV) in the PL spectrum of GQDs is a π-π* transition; it indicates the presence of sp^2 covalent bonds. However, the origin of the strong visible-light emission from GQDs ascribed to emissive surface traps and/or edge states remains unclear. In the absorption spectra of GQDs, it is widely accepted that absorption peaks in the visible range might originate from the electronic transitions of n-π* [41] surface states, which energy levels lie between the π and π* states of C=C [42,43] induced by various functional groups of C-OH, C=O, O-C=O, and C=N during the preparation of GQDs.

GQDs were synthesized by chemical oxidation and cutting of mm-pitch-based carbon fibers and exhibited a relatively narrow size distribution of 1-4 nm [44]. The GQDs synthesized at 120, 100, and 80 °C exhibit blue (approximately 400 nm), green (approximately 500 nm), and yellow (approximately 575 nm) emissions as shown Fig. 6(b). This result suggests that the various color emissions originate from differences in size. Fig. 6(c) represents the relationship between the size and energy gap, which decreases from 3.90 eV to 2.89 eV with increasing size and correlates with the quantum confinement effect for smaller QDs.

Recently, Kim *et al.* reported that the anomalous visible light luminescence from GQDs was strongly dependent on their size and shape [45]. They fabricated GQDs by the hydrothermal and chemical tailoring of graphene sheets obtained by thermal deoxidization of graphene oxide (GO) sheets produced from natural graphite powder using a modified Hummers method. The size of the GQDs (diameter *d*) was controlled by filtering and dialysis. The average sizes (d_a) were accurately estimated from the high-resolution transmission electron microscope (HRTEM) images for six types of samples with *d* ranging from 5 nm to 35 nm at each *d* and are indicated in the parentheses at the bottom of Fig. 7. For GQDs with d_a=5 and 12 nm, a single broad asymmetric PL peak centered at approximately 410 nm is observed. In particular, for GQDs with d_a = 17 and 22 nm, the PL spectra are resolved into two PL bands centered at approximately 415 and 505 nm, regardless of the excitation wavelength. This may be attributed to the combination of GQDs of different sizes/shapes. For GQDs with d_a=27 and 35 nm, the PL peak shape and position are restored to a single broad peak at approximately 410 nm, and the intensity of the PL peak for d_a=35 nm weakens considerably.

2.2.2 GO-QDs

Chien et al. [46] suggested a PL emission mechanism for GO and reduced GO (rGO), where GO was synthesized using the modified Hummers' method and xenon flash under ambient conditions. GO typically contains a large fraction of sp^3 hybridized carbon atoms bonded with epoxy, hydroxyl, carboxyl, and carbonyl oxygen functional groups, making it an electrical insulator. As shown in Fig. 8(a), two prominent and broad peaks are observed: P1 peak centered at approximately 600 nm and a

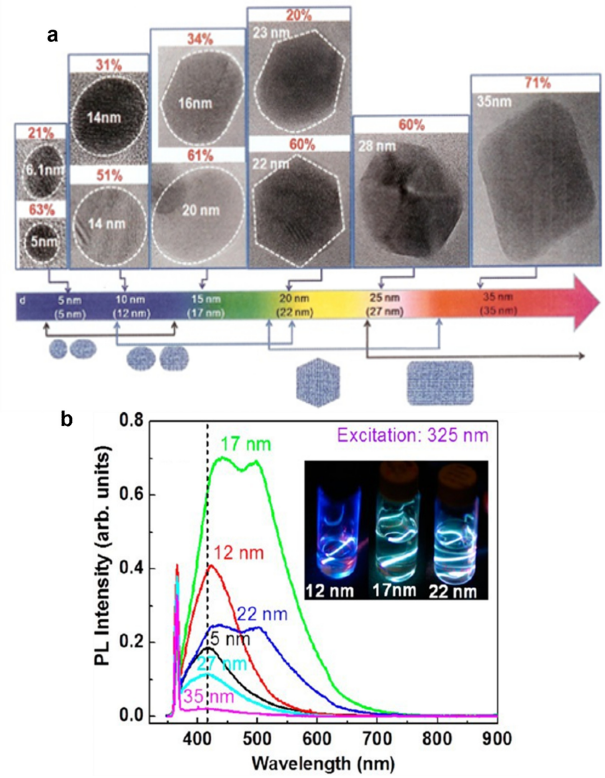

Fig. 7. (a) HRTEM images of GQDs with the increase of average size. (b) Size-dependent PL spectra for GQDs of 5-35 nm. Reprinted with permission from Ref. [45] Copyright (2012) ACS Publications.

small P2 emission peak centered at approximately 470 nm. P1 gradually decreases, whereas the P2 emission increases with increasing reduction exposure times.

Eda *et al.* reported the dependence of the HOMO–LUMO gap on the size of the GQDs [47]. Based on density functional theory (DFT), the energy gap of π-π^* decreases from 7 eV to 2 eV as the number (N) of aromatic rings increases from N=1 to 40. As shown in Fig. 9, the variation of the relative intensity ratios of the PL emission from the two different types of electronically excited states is suggested by the change in the heterogeneous electronic structures of GO and rGO with variable sp^2 and sp^3 hybridizations through reduction. The number of disorder-induced defect states in GO within the π–π^* gap decreased after deoxygenation. Additional cluster-like states were created from the newly formed small and isolated sp^2 domains, which increased the blue fluorescence at shorter wavelengths.

2.3 2D transitional metal dichalcogenide (TMD)

Since the discovery of 2D graphene, various 2D vdWs materials, such as hexagonal boron nitride (h-BN), black

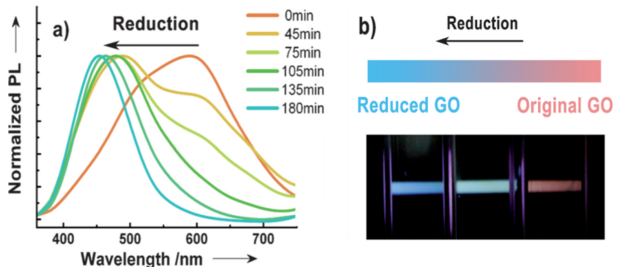

Fig. 8. (a) Normalized PL spectra of GO suspension and (b) photograph of tunable PL emission from GO at different reduction time. Reprinted with permission from Ref. [46] Copyright (2012) Wiley.

phosphorus (BP), and TMDs, have emerged as new candidates for overcoming the limitations for application to LEDs owing to the gapless and semi-metallic nature of graphene. h-BN, which has a large bandgap of approximately 6 eV, is a good insulator, and layered BP increases the bandgap to approximately 2 eV. Moreover, 2D TMDs with the formula MX_2 (M = Mo, W; X = S, Se, Te) have energy bandgaps covering the visible and near infrared spectral regions (1.0–2.1 eV). These can be extended to various photonic and optoelectronic applications, such as light-emitting devices, transistors, photovoltaic devices, and nanocavity lasers. However, they cannot be extended to blue emission. Compared with 2D TMDs, 0D TMDs possess higher bandgaps, ultrasmall sizes, high surface-to-volume ratios, and more active edge sites per unit mass, and thus can be mainly classified as QDs, NDs [48-50], (NPs) [51,52], small nanoflakes [53,54], and nanoplates [55].

In particular, the strong quantum confinement effect further promotes the characteristic PL of 0D TMDs. The 0D WS2 QDs exhibit blue emission at approximately 461 nm at a UV excitation of 310-380 nm as shown in Fig. 10(a), which is generated from

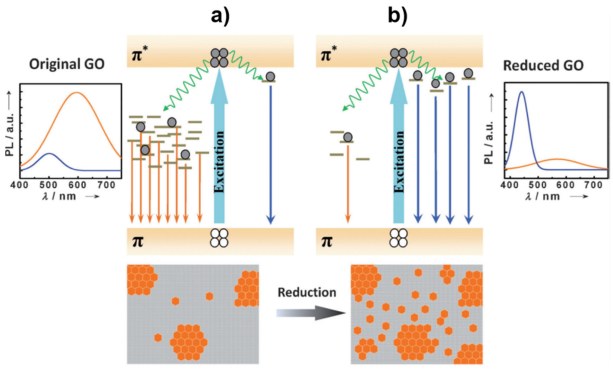

Fig. 9. Proposed PL mechanism of (a) the predominant IP1 and (b) predominant IP2 emission in GO. Reprinted with permission from Ref. [47] Copyright (2010) Wiley.

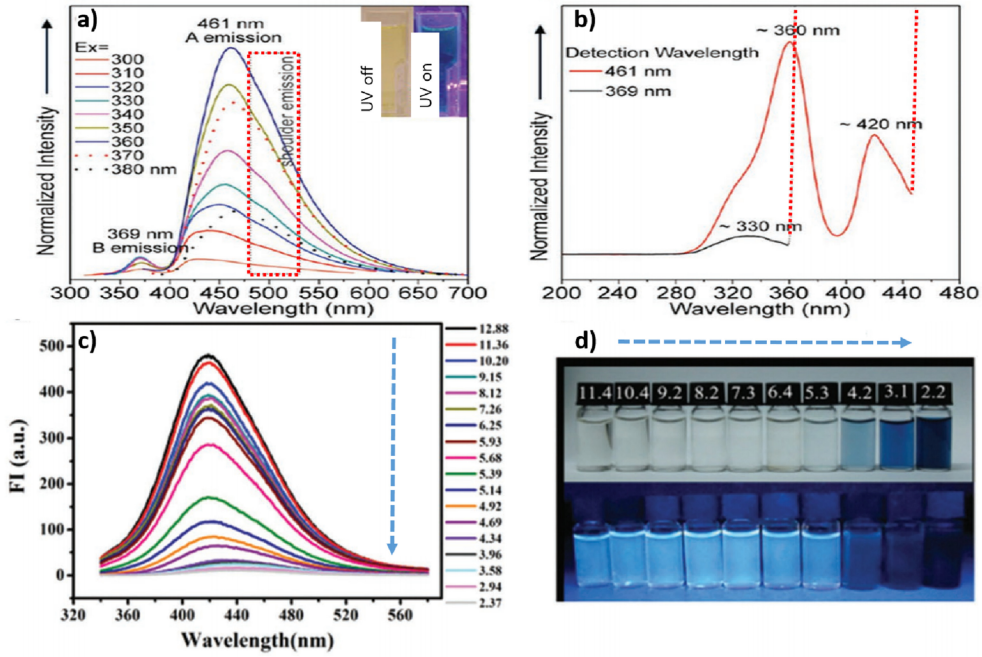

Fig. 10. (a) PL spectra of WS_2 QDs. (b) PLE spectra of WS_2 QDs. Reprinted with permission from Ref. [57] Copyright (2013) ACS Publications. (c) Fluorescent emission spectra of MoS_2 QDs at various pH values. (d) The photographs of resultant MoS_2 QDs solutions at various pH values under room (top) and 365 nm irradiation light (down). Reprinted with permission from Ref. [58] Copyright (2016) Royal Society of Chemistry.

the excitation of 360 and 420 nm energy levels as shown in Fig. 10(b). The pH-sensitive PL of the 0D MoS_2/WS_2 QDs is another interesting result. As shown in Fig. 10(c), the blue fluorescence intensity at approximately 420 nm from 0D MoS_2 QDs gradually decreases as the pH varies from 12.88 to 2.37. This is because the change in pH alters the microstructure of 0D MoS_2 QDs and agglomeration at low pH.

2.4 Hybrid QDs

2.4.1 ZnO/GQDs and ZnO/GO QDs.

Son et al. [58] first reported blue-emissive ZnO/GQD hybrid QDs. ZnO QDs hydrothermally synthesized using a Zn acetate dihydrate precursor were hybridized in N,N-Dimethylformamide (DMF) with GQDs exfoliated from graphite powder and treated using a mixture of H_2SO_4 and HNO_3. From the PL of quasi-core-shell ZnO/GQD hybrid QDs, the occurrence of blue luminescence (BL) at approximately 430 nm with a simultaneous decrease in near-band-edge emission intensity was first observed and sufficiently explained by the electronic transition from LUMO and LUMO+2, including the s-orbitals of GQDs, to O2p states of inner ZnO QDs (Fig. 11 (a), (b)). Similarly, Kim et al. [59] reported that when ZnO QDs synthesized by solution precipitation were hybridized with GO-QDs, the ZnO/GO-QDs exhibited blue emission irrespective of the excitation wavelength (Fig. 11(c), (d)). The first demonstration of excitation wavelength-independent blue emission was explained by the reduction of oxygen vacancy (V_o) defects in ZnO QDs owing to the formation of Zn-O-C bonds at the interface. The electronic energy Anderson diagram for the ZnO QDs was established based on the UV-Vis absorption spectra, PL, photoluminescence excitation (PLE), and ultraviolet photoemission spectroscopy results. According to this diagram, yellow luminescence (YL) occurring by the electronic transition from conduction band (CB) or Zn_i to V_o in ZnO QDs completely disappears, whereas only blue emission results from the electronic transition from either Zn_i or ex-Zn_i to V_{Zn} or from O-induced energy levels to V_{Zn}.

2.4.2. ZnO/f-PAHs

PAHs are small molecules with different numbers (n) of benzene rings. For n=2–5, their bandgaps and energy proximities resemble those of ZnO [60,61]. For hybridization with ZnO QDs containing Zn-OH bonds, two functionalized PAHs (f-PAHs) such as 2-naphthalene-5-sulfonic acid (5-ANSA) with amine (-NH_2) and sulfonic (-SO_3) functional groups [62], and 1-aminopyrene (1-PyNH_2) with amine groups

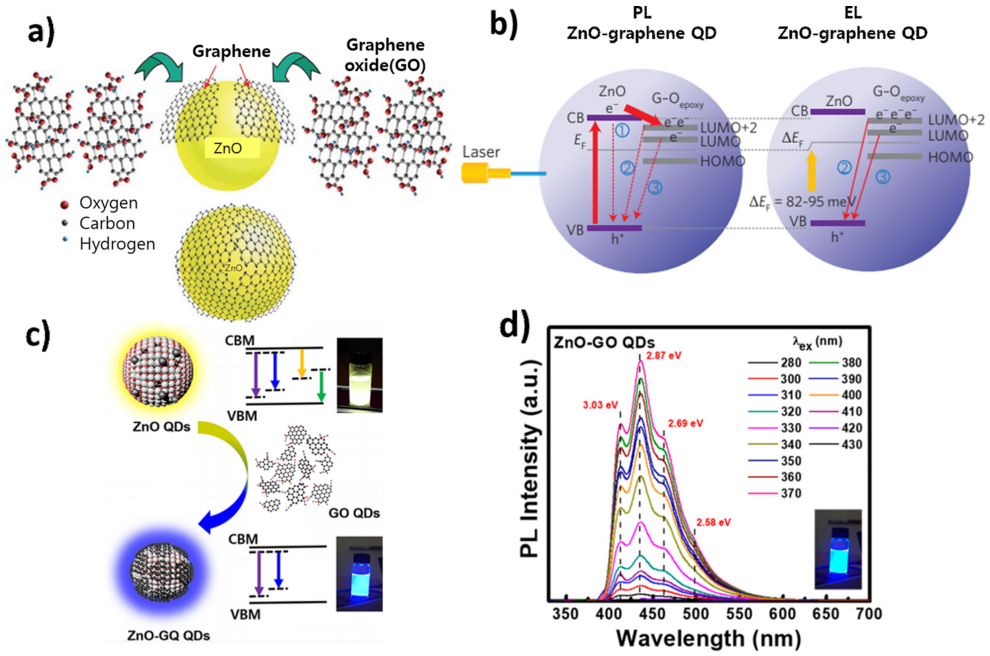

Fig. 11. (a) ZnO/GQDs structure (b) PL and EL mechanism in ZnO QDs and ZnO/GO-QDs. Reprinted with permission from Ref. [56] Copyright (2012) Nature Publishing Group. (c) YL from ZnO QDs and BL from ZnO/GO-QDs (d) Excitation independent PL of ZnO/GO-QDs. Reprinted with permission from Ref. [59] Copyright (2021) ACS Publications.

[63] were chosen. The formation of Zn-NH bonds after dehydration at the interface and the induced defect levels of 5-ANSA related to N, S, and O atoms and 1-PyNH$_2$ related to N were calculated using DFT (Gaussian 09 software package). The energy level hierarchy of the C=O, C=N, and C=S antibonding defect states is in order and located below the C=C antibonding (π^*) LUMO level. An electronic energy-band diagram was extracted from the results, as shown in Fig. 12. Using Fig. 12(a), the ZnO/ANSA and ZnO/1-PyNH$_2$ hybrid QDs were classified as type-II and quasi-type-II QDs, respectively. According to the energy diagram, blue emission is attributed to electronic transitions from both the O, N, S-induced anti-bonding (π^*) state to the O,N,S, bonding (π) state, ex-Zn$_i$ to V$_{Zn}$ of ZnO in type II ZnO/ANSA QDs, and the C=N anti-bonding (π^*) to the C=C bonding (π) state in ZnO/1-PyNH$_2$ quasi-type II QDs. Fig. 12(b) shows the electronic energy diagram of indium tin oxide (ITO)/ poly(3,4- ethylenedioxythiophene) : poly(styrenesulfonate) (PEDOT:PSS)/TFB/ZnO/1-PyNH$_2$// TPBi/LiF/Al QD-LEDs.

A deep-blue EL peak was observed at approximately 441 nm (FWHM= 42 nm) with 1931 CIE coordinates (0.17, 0.19). The EL device exhibited a turn-on voltage of 4 V, a luminance of 3379 cd/m^2 at 9.6 V, a current efficiency of 3.32 cd/A, and an EQE of 2.35% at 5.1 V. From the expected lifetime measurement, T50 at 100 cd/m^2 was estimated as 17830 h with an acceleration factor of n=1.2, which is smaller than the value of n=1.5 for ZnTeSe blue QD-based EL devices, implying slow degradation [26].

2.5 PQDs

Halogenated perovskites (ABX$_3$) are metal oxides with a special structure, which exhibit the properties of insulators, semiconductors, and conductors, as well as superconductivity. Here, A, B, and C represent a monovalent organic or inorganic cation, divalent metal cation (Pb or Sn), and halogen anion (I, Br, or Cl), respectively. The structural stability from the ionic radii of A, B, and X (rA, rB, rX) is determined by the Goldschmidt acceptance factor (t), t=(rA+rX/($\sqrt{}$2(rB+rX)) (0.8<t<0.9). PQDs have a high recombination probability, wide color gamut (130%), and high PLQY of over 80%. The emission band and thermal stability can be controlled by changing the halide type and type of cation, respectively. In addition to the above advantages of PQDs, the low cost of solution-based manufacturing favors perovskite LEDs (PeLEDs) [64,65]. However, their intrinsic drawbacks, especially with regard to their instability and large-scale synthesis, deserve close attention [66]. The state-of-the-art synthesis and progress in research on PQD-based LEDs are reviewed in Ref. [67] Since the first report on the synthesis of CsPbX$_3$ PQDs, that exhibit bright emission and a wide color gamut, using the hot injection method by Loredana et al [68,69] (Fig. 13(a)), inorganic

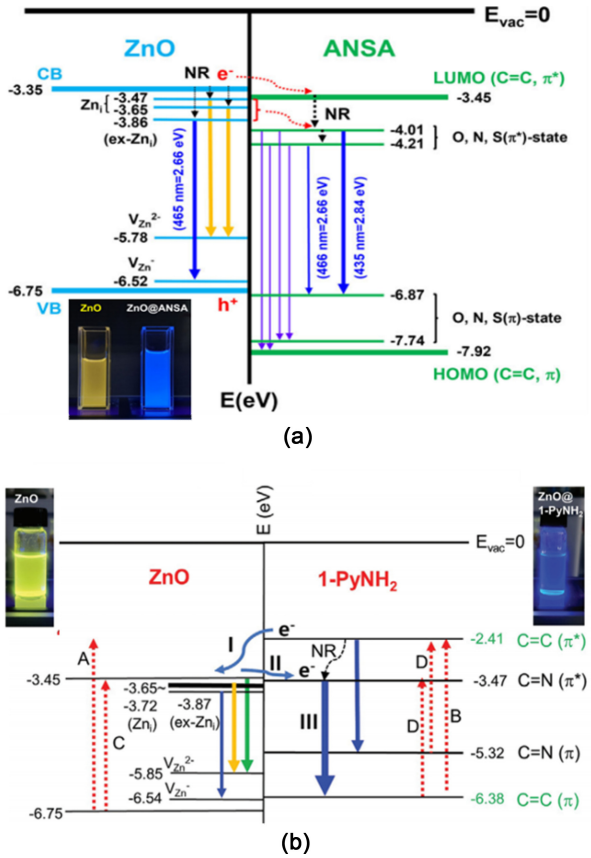

Fig. 12. (a) Electronic band diagram and PL mechanism of ZnO and ZnO and ZnO/ANSA QDs. Reprinted with permission from Ref. [62] Copyright (2022) Wiley and (b) those of ZnO and ZnO/1-PyNH$_2$ QDs. Reprinted with permission from Ref. [63] Copyright (2022) Wiley.

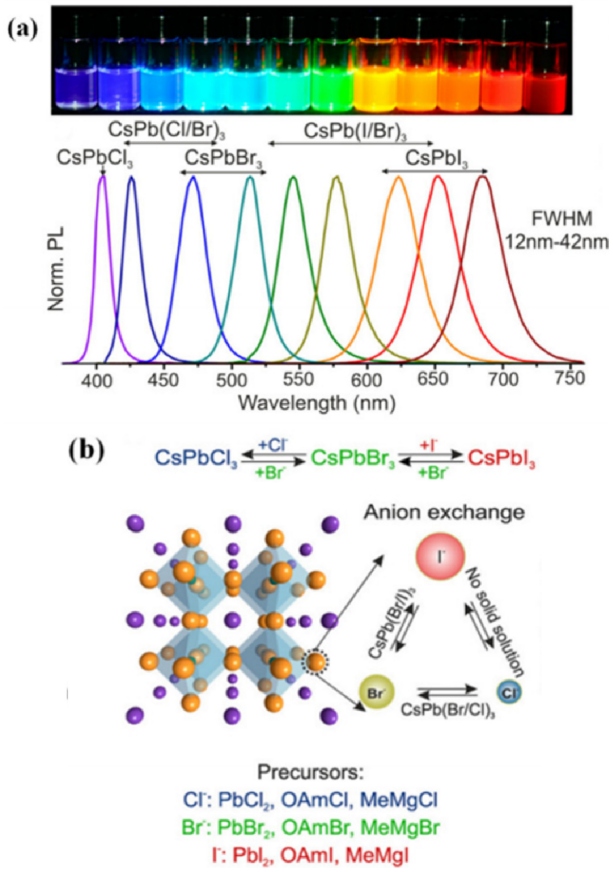

Fig. 13. (a) Colloidal perovskite $CsPbX_3$ PQDs (X = Cl, Br, I) covering a whole visible spectral wavelength. Reprinted with permission from Ref. [69] Copyright (2015) ACS Publications. (b) The anion exchange diagram. Reprinted with permission from Ref. [70] Copyright (2016) Wiley.

PQDs (IPQDs) obtained by introducing different halogen elements into $CsPbX_3$ QDs for an anion exchange reaction (Fig. 13 (b)) [68], microwave-assisted [70,71] synthesis of $CsPbX_3$ nanocrystals (NCs) with different morphologies [69,72], and $CsPbX_3$ microcrystals using chemical vapor deposition [73] have been introduced. In recent years, the synthesis of various types of nanocrystals with good homogeneity using a fully automated microfluidic platform has been actively studied [65,74]. Although PQDs exhibit a high PLQY, low Auger recombination loss, and large exciton binding energy, their poor humidity resistance and thermal stability greatly limit their practical application in the display field. To improve the performance of PQD-based PeLEDs (PeQLEDs), ion doping with A-, B-, and X-site doping; multiple ion doping; typical ligand modification; and coating engineering have been adopted. Compared with ion doping and ligand modification strategies, coating is a more straightforward encapsulation strategy for performance improvement by isolating as much water and oxygen as possible from the inner-core PQDs. Attempts have been made to apply PQDs to displays as PQDs backlight and color conversion layers, and PeLEDs as EL devices. In the former backlight and color conversion, green and red PQDs were primarily used as green and red emitters, respectively, in combination with blue OLED or micro-LEDs. Pan et al. [75] incorporated Ni^{2+} ions into $CsPbCl_xBr_{3-x}$ QDs by a supersaturated recrystallization synthetic method and modulated the Cl/Br element ratios to obtain an efficient blue PeQLEDs. The corresponding device exhibited a maximum luminance of 612 cd m^{-2} and EQE of 2.4% (Fig. 14(a)). Fig. 14(b) summarizes the EQE development of full-color PeQLED devices. To date, the maximum EQE values of red, green, and blue QLED have reached 21.6%, 23.4%, and 12.3%, respectively, which is an increase of approximately 20% since 2015. However, the lifetime of PeQLEDs is considerably shorter than the commercial standard of 10,000 h.

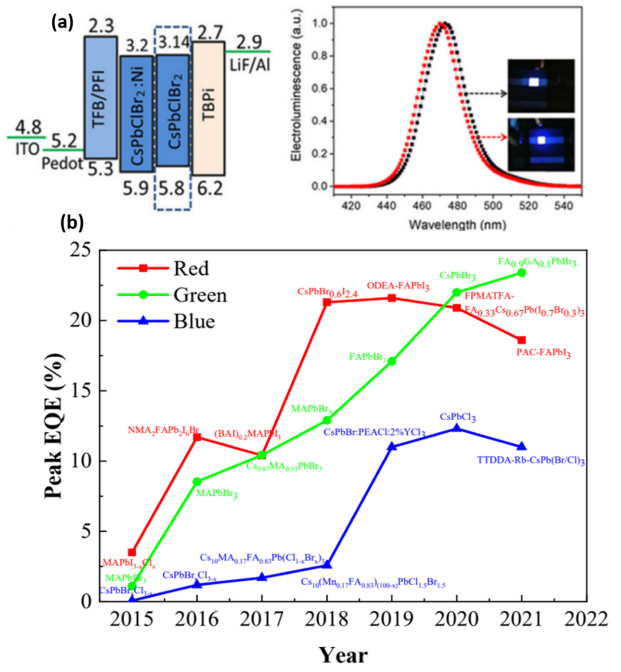

Fig. 14. (a) Band level of the PeQLEDs based on 2.5% Ni^{2+} ion-doped $CsPbCl_{0.99}Br_{2.01}$ QDs (left). The EL spectra and photos of the PeQLEDs based on $CsPbClBr_2$ QDs (black) and 2.5% Ni^{2+}-doped $CsPbCl_{0.99}Br_{2.01}$ QDs (red). Reprinted with permission from Ref. [75] Copyright (2020) ACS Publications. (b) Evolution curve of the peak EQE of perovskite QLEDs. Reprinted with permission from Ref. [67] Copyright (2022) MDPI.

3. CONCLUSIONS

QDs are the most suitable for future flexible and wearable displays, including formless displays, owing to their high color purity, brightness, large color gamut, and low driving voltage. The recent rapid progress in three-dimensional patterning techniques has facilitated the development of ultrahigh-resolution full-color QLEDs. To develop QLED-based futuristic displays, highly efficient and stable inorganic QDs comprising heavy and toxic metals should be replaced by highly efficient, non-toxic, and eco-friendly materials, and a mass production process should be well established in parallel. Both II-VI ZnO and ZnSe QDs are required to overcome this bottleneck. For ZnO QDs, synthetic methods (chemical or physical) for producing highly crystalline and well-passivated ZnO QDs displaying only near-band-edge emission must be found before applying in UV excitation source as well as fabricating ZnO(S, Se) alloy for a blue emitter. For ZnSe QDs, a secure and reproducible process for synthesizing blue-emissive ZnSe alloys with core-shell-shell structures is required. The environmental instability of PeQLEDs is the main obstacle to their commercialization. Consequently, improving the performance and stability of PQDs and developing passivation techniques with ultrahigh-barrier films remain the primary goals for future development.

ACKNOWLEDGMENT

This study was partially supported by the KIST Institutional Program.

REFERENCES

[1] B. Zhao, Q. Wang, D. Li, H. Yang, X. Bai, S. Li, P. Liu, and X. Sun, “Red and green quantum dot color filter for Full-Color Micro-LED arrays”, *Micromachines*, Vol. 13, No. 4, pp. 595-601, 2022.

[2] Z. Yang, M. Gao, W. Wu, X. Yang, X. W. Sun, J. Zhang, H. Wang, R. Liu, C. Han, H. Yang, and H. Li, “Recent advances in quantum dot-based light-emitting devices: Challenges and possible solutions”, *Mater. Today*, Vol. 24, pp. 69-93, 2019.

[3] D. A. Hanifi, N. D. Bronstein, B. A. Koscher, Z. Nett, J. K. Swabeck, K. Takano, A. M. Schwartzberg, L. Maserati, K. Vandewal, Y. van de Burgt, A. Salleo, and A. P. Alivisatos, “Redefining near-unity luminescence in quantum dots with photothermal threshold quantum yield”, *Science*, Vol. 363, No. 6432, pp. 1199-1202, 2019.

[4] O. Chen, J. Zhao, V. P. Chauhan, J. Cui, C. Wong, D. K. Harris, H. Wei, H. Han, D. Fukumura, R. K. Jain, and M. G. Bawendi, “Compact high-quality CdSe-CdS core-shell nanocrystals with narrow emission linewidths and suppressed blinking”, *Nat. Mater.*, Vol. 12, No. 5, 445-451, 2013.

[5] Y. Won, O. Cho, T. Kim, D. Chung, T. Kim, H. Chung, H. Jang, J. Lee, D. Kim, and E. Jang, “Highly efficient and stable InP/ZnSe/ZnS quantum dot light-emitting diodes”, *Nature*, Vol. 575, No. 7784, pp. 634-638. 2019.

[6] Y. Kim, S. Ham, H. Jang, J.H. Min, H. Chung, J. Lee, D. Kim, and E. Jang, “Bright and uniform green light emitting InP/ZnSe/ZnS quantum dots for wide color gamut displays”, *ACS Appl. Nano Mater.*, Vol. 2, No. 3, pp. 1496-1504, 2019.

[7] R. J. Ellingson, M. C. Beard, J. C. Johnson, P. Yu, O. I. Micic, A. J. Nozik, A. Shabaev, and A. L. Efros, “Highly Efficient Multiple Exciton Generation in Colloidal PbSe and PbS Quantum Dots”, *Nano Lett.*, Vol. 5, No. 5, pp. 865-871, 2005.

[8] R. Muñoz, E. M. Santos, C. A. Galan-Vidal, J. M. Miranda, A. Lopez-Santamarina, and J. A. Rodriguez, “Ternary Quantum Dots in Chemical Analysis. Synthesis and Detection Mechanisms”, *Molecules*, Vol. 26, No. 9, pp. 2764-2779, 2021.

[9] C. M. Doneg, P. Liljeroth, and D. Vanmaekelbergh, “Phys-

icochemical Evaluation of the Hot-Injection Method, a Synthesis Route for Monodisperse Nanocrystals", *Small*, Vol. 1, No. 12, pp. 1152-1162, 2005.

[10] F. Einar Kruis, H. Fissan, A. P. Agarwal, H. Rai, and S. Mondal, "Synthesis of Nanoparticles in the gas phase forl electronic, optical and magnetic applications-A Review", *J. Aerosol Sci.*, Vol. 29, No. 5-6, pp. 511-535, 1998.

[11] G. Li, Q. Li, R. Cheng, and S. Chen, "Synthesis of quantum dots based on microfluidic technology", *Curr. Opin. Chem. Eng.*, Vol. 29, pp. 34-41, 2020.

[12] S. Kubendhiran, Z. Bao, K. Dave, and R. Liu, "Micro-fluidic Synthesis of Semiconducting Colloidal Quantum Dots and Their Applications", *ACS Appl. Nano Mater.*, Vol. 2, No. 4, pp. 1773-1790, 2019.

[13] J. Yang, M. K. Choi, D. Kim, and T. Hyeon, "Designed assembly and integration of colloidal nanocrystals for device applications", *Adv. Mater.*, Vol. 28, No. 6, pp.1176-1207, 2016.

[14] X. Dai, Y. Deng, X. Peng, and Y. Jin, "Quantum-dot light-emitting diodes for large area displays: towards the dawn of commercialization", *Adv. Mater.*, Vol. 29, No. 14, p.1607022, 2017.

[15] S. Pimputkar, J. S. Speck, S. P. Denbaars, and S. Nakamura, "Prospects for LED lighting", *Nat. Photon.*, Vol. 3, No. 4, pp.180-182, 2009.

[16] Y. Yang, Y. Zheng, W. Cao, A. Titov, J. Hyvonen, J. R. Manders, J. Xue, P. H. Holloway, and L. Qian, "High-efficiency light-emitting devices based on quantum dots with tailored nanostructures", *Nat. Photonics*, Vol. 9, No. 4, pp. 259-266, 2015.

[17] H. Goesmann and C. Feldmann, "Nanoparticulate functional materials", *Angew. Chem. Int. Ed.*, Vol. 49, No. 8, pp. 1362-1395, 2010.

[18] L. Wang, J. Lin, Y. Hu, X. Guo, Y. Lv, Z. Tang, J. Zhao, Y. Fan, N. Zhang, Y. Wang, and X. Liu, "Blue Quantum Dot Light-Emitting Diodes with High Electroluminescent Efficiency", *ACS Appl. Mater. Interfaces*, Vol. 9, No. 44, pp. 38755-38760, 2017.

[19] C. Pu, X. Dai, Y. Shu, M. Zhu, Y. Deng, Y. Jin, and X. Peng, "Electrochemically-stable ligands bridge the photoluminescence-electroluminescence gap of quantum dots", *Nat. Commun.*, Vol. 11, No. 1, pp. 937-946, 2020.

[20] L. Qian, Y. Zheng, J. Xue, and P. H. Holloway, "Stable and Efficient Quantum-Dot Light-Emitting Diodes Based on Solution Multilayer Structures", *Nat. Photon.*, Vol. 5, No. 9, pp. 543-548, 2011.

[21] J. Kwak, W. K. Bae, D. Lee, I. Park, J. Lim, M. Park, H. Cho, H. Woo, D. Y. Yoon, K. Char, S. Lee, and C. Lee, "Bright and Efficient Full-Color Colloidal Quantum Dot Light-Emitting Diodes Using an Inverted Device Structure", *Nano Lett.*, Vol. 12, No. 5, pp. 2362-2366, 2012.

[22] K. Lee, J. Lee, W. Song, H. Ko, J. Lee, and H. Yang, "Highly Efficient, Color-Pure, Color-Stable Blue Quantum Dot Light-Emitting Devices", *ACS Nano*, Vol. 7, No. 8, pp. 7295-7302, 2013.

[24] J. P. Park, J. Lee, and S. Kim, "Highly luminescent InP/GaP/ZnS QDs emitting in the entire color range via a heating up process", *Sci. Rep.*, Vol. 6, No. 1, pp. 30094(1)-30094(6), 2016.

[25] H. Zhang, X. Ma, Q. Lin, Z. Zeng, H. Wang, L. S. Li, H. Shen, Y. Jia, and Z. Du, "High-Brightness Blue InP Quantum Dot-Based Electroluminescent Devices: The Role of Shell thickness", *J. Phys. Chem. Lett.*, Vol. 11, No. 3, pp. 960-967, 2020.

[26] T. Kim, K.-H. Kim, S. Kim, S.-M. Choi, H. Jang, H.-K. Seo, H. Lee, D.-Y. Chung, and E. Jang, "Efficient and stable blue quantum dot light-emitting diode", *Nature*, Vol. 586, pp. 385-389, 2020.

[27] S. Jain, S. Bharti, G. K. Bhullar, and S. K. Tripathi, "I-III-VI core/shell QDs: Synthesis, characterizations and applications", *J. Lumin.*, Vol. 219, pp. 116912-11630, 2020.

[28] T. S. Ponomaryovaa A. S. Novikovaa, A. M. Abramovaa, O. A. Goryachevaa, D. D. Drozda, P. D. Strokina, and I. Yu. Goryachevaa, "New-Generation Low-Toxic I–III–VI2 Quantum Dots in Chemical Analysis", *J. Anal. Chem.*, Vol. 77, No. 4, pp. 402-409, 2022.

[29] K. Zheng, M. I. Setyawati, T. P. Lim, D. T. Leong, and J. Xie, "Antimicrobial Cluster Bombs: Silver Nanoclusters Packed with Daptomycin", *ACS Nano.*, Vol. 10, No. 8, pp. 7934-7942, 2016.

[30] N. Goswami, F. Lin, Y. Liu, D. T. Leong, and J. Xie, "Highly Luminescent Thiolated Gold Nanoclusters Impregnated in Nanogel", *Chem. Mater.*, Vol. 28, pp. 4009-4016, 2016.

[31] X. Hu, T. Liu, Y. Zhuang, W. Wang, Y. Li, W. Fan, Y. Huang, "Recent advances in the analytical applications of copper nanoclusters", *TrAC Trend Anal. Chem.*, Vol. 77, pp. 66-75, 2016.

[32] S. L. Chia, C. Y. Tay, M. I. Setyawati, and D. T. Leong, "Decoupling the Direct and Indirect Biological Effects of ZnO Nanoparticles Using a Communicative Dual Cell-Type Tissue Construct", *Small*, Vol. 12, No. 5, pp. 647-657, 2016.

[33] M. Olutas, B. Guzelturk, Y. Kelestemur, K. Gungor, and H. V. Demir, "Noncontact Temperature Probing: Highly Efficient Nonradiative Energy Transfer from Colloidal Semiconductor Quantum Dots to Wells for Sensitive Noncontact Temperature Probing", *Adv. Funct. Mater.*, Vol. 26, No. 17, pp. 2891-2899, 2016.

[34] X. T. Zheng, A. Ananthanarayanan, K. Q. Luo, and P. Chen, "Glowing Graphene Quantum Dots and Carbon Dots: Properties, Syntheses, and Biological Applications", *Small*, Vol. 11, No. 14, pp. 1620-1636, 2015.

[35] B. Kong, J. Tang, Y. Zhang, T. Jiang, X. Gong, C. Peng, J. Wei, J. Yang, Y. Wang, X. Wang, G. Zheng, C. Selomulya, and D. Zhao, "Incorporation of well-dispersed sub-5-nm graphitic pencil nanodots into ordered mesoporous frameworks", *Nat. Chem.*, Vol. 8, No. 2, pp. 171-178, 2016.

[36] S. Qu, D. Zhou, D. Li, W. Ji, P. Jing, D. Han, L. Liu, H. Zeng, and D. Shen, "Toward Efficient Orange Emissive Carbon Nanodots through Conjugated sp2-Domain Controlling and Surface Charges Engineering", *Adv. Mater.*, Vol. 28, No. 18, pp. 3516-3521, 2016.

[37] Y. Wu, X. Zhu, X. Ji, W. Liu, W. Wan, Y. Wang, X. Pan, and Z. Lu, "Graphene quantum dots as a highly efficient electrocatalyst for lithium–oxygen batteries", *J. Mater. Chem. A*, Vol. 8, No. 42, pp. 22356-22368, 2020.

[38] J. Robertson and E. P. O'Reilly, "Electronic and atomic structure of amorphous carbon", *Phys. Rev. B*, Vol. 35, No. 6, pp. 2946-2957, 1987.
[39] C. Mathioudakis, G. Kopidakis, P.C. Kelires, P. Patsalas, M. Gioti, and S. Logothetidis, "Electronic and optical properties of a-C from tight-binding molecular dynamics simulations", *Thin Solid Films*, Vol. 482, No. 1-2, pp.151-155, 2005.
[40] C. W. Chen and J. Robertson, "Nature of disorder and localization in amorphous carbon", *J. Non-Cryst. Solids*, Vol. 227-230, pp. 602-606, 1998.
[41] S. J. Zhu, S. J. Tang, J. H. Zhang, and B. Yang, "The photoluminescence mechanism in carbon dots (graphene quantum dots, carbon nanodots, and polymer dots): Current state and future perspective", *Chem. Commun.*, Vol. 48, pp. 4527-4539, 2012.
[42] L. Tang, R. Ji, X. Cao, J. Lin, H. Jiang, X. Li, K. S. Teng, C. M. Luk, S. Zeng, J. Hao, and S. P. Lau, "Deep Ultraviolet Photoluminescence of Water-Soluble Self-Passivated Graphene Quantum Dots", *ACS Nano*, Vol. 6, No. 6, pp. 5102-5110, 2012.
[43] Y. Zhou, Q. Bao, L. A. L. Tang, Y. Zhong, and K. P. Loh, "Hydrothermal dehydration for the "green" reduction of exfoliated graphene oxide to graphene and demonstration of tunable optical limiting", *Chem. Mater.*, Vol. 21, No. 13, pp. 2950-2956, 2009.
[44] J. Peng, W. Gao, B. K. Gupta, Z. Liu, R. Romero-Aburto, L. Ge, L. Song, L. B. Alemany, X. Zhan, G. Gao, S. A. Vithayathil, B. A. Kaipparettu, A. A. Marti, T. Hayashi, J. Zhu, and P. M. Ajayan, "Graphene quantum dots derived from carbon fibers", *Nano Lett.*, Vol. 12, pp. 844-849, 2012.
[45] S. Kim, S. W. Hwang, M. K. Kim, D. Y. Shin, D. H. Shin, C. O. Kim, S. B. Yang, J. H. Park, E. Hwang, S. K. Choi, G. Ko, S. Sim, C. Sone, H. J. Choi, S. Bae, and B. H. Hong, "Anomalous behaviors of visible luminescence from graphene quantum dots: Interplay between size and shape", *ACS Nano*, Vol. 6, No. 9, pp. 8203-8208, 2012.
[46] C. T. Chien, S. S. Li, W. J. Lai, Y. C. Yeh, H. A. Chen, I. S. Chen, L. C. Chen, K. H. Chen, T. Nemoto, S. Isoda, M. Chen, T. Fujita, G. Eda, H. Yamaguchi, M. Chhowalla, and C. W. Chen, "Tunable Photoluminescence from Graphene Oxide", *Angew. Chem. Int. Ed.*, Vol. 51, No. 27, pp. 6662-6666, 2012.
[47] G. Eda, Y.-Y. Lin, C. Mattevi, H. Yamaguchi, H.-A. Chen, I.-S. Chen, C.-W. Chen, and M. Chhowalla, "Blue photoluminescence from chemically derived graphene oxide", *Adv. Mater.*, Vol. 22, No. 4, pp. 505-509, 2010.
[48] K. P. Loh, Q. Bao. G. Eda, and M. Chhowalla, "Graphene oxide as a chemically tunable platform for optical applications", *Nat. Chem.*, Vol. 2, No. 12, pp. 1015-1024, 2010.
[49] Q. S. Mei, K. Zhang, G. J. Guan, B. H. Liu, S. H. Wang, and Z. P. Zhang, "Highly efficient photoluminescent graphene oxide with tunable surface properties", *Chem. Commun.*, Vol. 46, No. 39, pp. 7319-7321, 2010.
[50] H. Min, J. E. Hill, N. A. Sinitsyn, B. R. Sahu, L. Kleinman, and A. H. MacDonald, "Intrinsic and Rashba spin-orbit interactions in graphene sheets", *Phys. Rev. B*, Vol. 74, No. 16, pp. 165310(1)- 165310(5), 2006.
[51] J. R. Petta, A. C. Johnson, J. M. Taylor, E. Laird, A. Yacoby, M. D. Lukin, C. M. Marcus, M. P. Hanson, and A. C. Gossard, "Coherent Manipulation of Coupled Electron Spins in Semiconductor Quantum Dots", *Science*, Vol. 309, No. 5744, pp. 2180-2184, 2005.
[52] F. H. L. Koppens, C. Buizert, K. J. Tielrooij, I. T. Vink, K. C. Nowack, T. Meunier, L. P. Kouwenhoven, and L. M. K. Vandersypen, "Driven coherent oscillations of a single electron spin in a quantum dot", *Nature*, Vol. 442, No. 7104, pp. 766-771, 2006.
[53] S. N. Baker and G. A. Baker, "Luminescent Carbon Nanodots: Emergent Nanolights", *Angew. Chem. Int. Ed.*, Vol. 49, No. 38, pp. 6726-6744, 2010.
[54] X. Yan, X. Cui, and X. Li, "Synthesis of large, stable colloidal graphene quantum dots with tunable size", *J. Am. Chem. Soc.*, Vol. 132, No. 17, pp. 5944-5945, 2010.
[55] X. Yan, B. Li, and L. Li, "Colloidal Graphene Quantum Dots with Well-Defined Structures", *Acc. Chem. Res.*, Vol. 46, No. 10, pp. 2254-2262, 2013.
[56] D. I. Son, B. W. Kwon, D. H. Park, W.-S. Seo, Y. Yi, B. Angadi, C.-L. Lee, and W. K. Choi, "Emissive ZnO-graphene quantum dots for white-light-emitting diodes", *Nat. Nanotechnol.*, Vol. 7, No. 7, pp. 465-471, 2012.
[57] L. Lin, Y. Xu, S. Zhang, I. M. Ross, A. C. Ong, and D. A. Allwood, "Fabrication of Luminescent Monolayered Tungsten Dichalcogenides Quantum Dots with Giant Spin-Valley Coupling", *ACS Nano*, Vol. 7, No. 9, pp. 8214-8223, 2013.
[58] S. Zhang, X. Jia, and E. Wang, "Facile synthesis of optical pH-sensitive molybdenum disulfide quantum dots", *Nanoscale*, Vol. 8, No. 33, pp. 15152-15157, 2016.
[59] H. H. Kim, Y. Lee, Y. J. Lee, J. Jeong, Y. Yi, C. Park, S.-Y. Yim, B. Angadi, K.-J. Ko, J.-W. Kang, and W. K. Choi, "Realization of Excitation Wavelength Independent Blue Emission of ZnO Quantum Dots with Intrinsic Defects", *ACS Photonics*, Vol. 7, No. 3, pp.723-734, 2021.
[60] R. Shimada, B. Urban, M. Sharma, A. Singh, V. Avrutin, H. Morkoç, and A. Neogi, "Energy transfer in ZnO-anthracene hybrid structure", *Opt. Mater. Express*, Vol. 2, No. 4, pp. 526-533, 2012.
[61] A. Menson, J. A. H. Jochen, J. W. Martin, J. Akroyd, J. Robertson, and M. Kraft, "Optical band gap of cross-linked, curved, and radical polyaromatic hydrocarbons", *Phys. Chem. Chem. Phys.*, Vol. 21, No. 29, pp. 16240-16251, 2019.
[62] H. H. Kim, S. Park, H. Lee, J. K. Kang, and W. K. Choi, "Blue-Light Emissive Type II ZnO@5-Amino-2-Naphthalene Sulfonic Acid Core–Shell Quantum Dots", *Adv. Photon. Res.*, Vol. 3, No. 4, pp. 2100315-2100327, 2022.
[63] H. H. Kim, S. Park, K.-J. Ko, S.-Y. Yim, J.-W. Kang, and W. K. Choi, "Blue Light Emitting Diodes based on Bright Quasi-Type-II ZnO@1-Aminopyrene Hybrid Quantum Dots with a Long Operation Life", *Adv. Opt. Mater.*, Vol. 10, No. 18, pp. 2200601-2200611, 2022.
[64] A. Swarnkar, R. Chulliyil, V. K. Ravi, M. Irfanullah, and A. Chowdhury, "Colloidal CsPbBr3 Perovskite Nanocrystals: Luminescence beyond Traditional Quantum Dots", *Angew. Chem. Int. Ed.*, Vol. 54, pp. 15424-15428, 2015.
[65] J. Wang, X. Liu, L. Zhou, W. Shen, M. Li, and R. He,

"Highly luminescent and stable quasi-2D perovskite quantum dots by introducing large organic cations", *Nanoscale Adv.*, Vol. 3, No. 18, pp. 5393-5398, 2021.

[66] W. Lv, L. Li, M. Xu, J. Hong, X. Tang, L. Xu, Y. Wu, R. Zhu, R. Chen, and W. Huang, "Improving the stability of metal halide perovskite quantum dots by encapsulation", *Adv. Mater.*, Vol. 31, No. 28, p.1900682, 2019.

[67] X. Ren, X. Zhang, H. Xie, J. Cai, C. Wang, E. Chen, and S. Xu, "Perovskite Quantum Dots for Emerging Displays: Recent Progress and Perspectives", *Nanomaterial*, Vol. 12, No. 13, pp. 2243-2270, 2022.

[68] G. Nedelcu, L. Protesescu, S. Yakunin, M.I. Bodnarchuk, M. J. Grotevent, and M. V. Kovalenko, "Fast Anion-Exchange in Highly Luminescent Nanocrystals of Cesium Lead Halide Perovskites (CsPbX3, X = Cl, Br, I)", *Nano Lett.*, Vol. 15, No. 8, pp. 5635-5640, 2015.

[69] L. Protesescu, S. Yakunin, M. I. Bodnarchuk, F. Krieg, R. Caputo, C. H. Hendon, R. X. Yang, A. Walsh, and M. V. Kovalenko, "Nanocrystals of cesium lead halide perovskites (CsPbX3, X = Cl, Br, and I): Novel optoelectronic materials showing bright emission with wide color gamut", *Nano Lett.*, Vol. 15, No. 6, pp. 3692-3696, 2015.

[70] X. Li, Y. Wu, S. Zhang, B. Cai, Y. Gu, J. Song, and H. Zeng, "CsPbX3 Quantum Dots for Lighting and Displays: Room-Temperature Synthesis, Photoluminescence Superiorities, Underlying Origins and White Light-Emitting Diodes", *Adv. Funct. Mater.*, Vol. 26, No. 15, pp. 2435-2445, 2016.

[71] I. Lignos, R. Maceiczyk, and A. J. de Mello, "Microfluidic Technology: Uncovering the Mechanisms of Nanocrystal Nucleation and Growth", *Acc. Chem. Res.*, Vol. 50, No. 5, pp. 1248-1257, 22017.

[72] M. Chen, Y. Zou, L. Wu, Q. Pan, D. Yang, H. Hu, Y. Tan, Q. Zhong, Y. Xu, H. Liu, B. Sun, and Q. Zhang, "Solvothermal Synthesis of High-Quality All-Inorganic Cesium Lead Halide Perovskite Nanocrystals:From Nanocube to Ultrathin Nanowire", *Adv. Funct. Mater.*, Vol. 27, No. 23, p. 1701121, 2017.

[73] I. Lignos, V. Morad, Y. Shynkarenko, C. Bernasconi, R. M. Maceiczyk, L. Protesescu, F. Bertolotti, S. Kumar, S. T. Ochsenbein, N. Masciocchi, A. Guagliardi, C.-J. Shih, M. I. Bodnarchuk, A. J. deMello, and M. V. Kovalenkom, "Exploration of Near-Infrared-Emissive Colloidal Multinary Lead Halide Perovskite Nanocrystals Using an Automated Microfluidic Platform", *ACS Nano*, Vol. 12, No. 6, pp. 5504-5517,2018.

[74] X. Li, F. Cao, D. Yu, J. Chen, Z. Sun, Y. Shen, Y. Zhu, L. Wang, Y. Wei, Y. Wu, and Haibo Zeng, "All inorganic halide perovskites nanosystem: Synthesis, structural features, optical properties and optoelectronic applications", *Small*, Vol. 13, No. 9, p.1603996. 2017.

[75] G. Pan, X. Bai, W. Xu, X. Chen, Y. Zhai, J. Zhu, H. Shao, N. Ding, L. Xu, B. Dong, Y. Mao, and H. Song, "Bright blue light emission of Ni2+ion-doped CsPbClxBr3-x perovskite quantum dots enabling efficient light-emitting devices", *ACS Appl. Mater. Interfaces*, Vol. 12, No. 12, pp. 14195-14202, 2020.